# Climate teleconnections, interannual variability and evolution of the rainfall regime in a tropical Caribbean island: case study of Barbados

Taha B.M.J. Ouarda[1,*], Christian Charron[1], Smail Mahdi[2] and Latifa A. Yousef[3]

[1]Canada Research Chair in Statistical Hydro-Climatology, INRS-ETE, 490 rue de la Couronne, Quebec, QC, G1K9A9, Canada.

[2]Department of Computer science, Mathematics and Physics, University of the West Indies, Cave Hill Campus, Barbados.

[3]The National Center of Meteorology, P.O. Box 4815, Abu Dhabi, UAE.

*Corresponding author: Dr. Taha B.M.J. Ouarda

Email: taha.ouarda@ete.inrs.ca

Tel: +1 418 654 3842

December 2020

## Abstract

A limited number of studies have focused on the hydroclimate dynamics of tropical Caribbean islands. The present study aims to analyze the rainfall regime in Barbados. CHIRPS gridded dataset, at a resolution of 0.05°×0.05°, providing daily rainfall data from January 1981 until 2018 was used. The variables analyzed were the annual and seasonal maximum rainfall; the total annual and seasonal rainfall; and the number of rainy days per year and per season. Potential change points in rainfall time-series were detected with a Bayesian multiple change point detection procedure. Time series were then analyzed for detection of trends using the modified Mann-Kendall test. The true temporal slopes of the rainfall time series were obtained with the Theil-Sen's statistic. The links between rainfall and various global climate oscillation indices were also investigated. Results indicate that no change points or significant trends were observed in the annual rainfall time series. However, it was found that some climate indices have a strong correlation with precipitation on the island, especially for the total rainfall and the number of rainy days. A stationary and non-stationary frequency analysis is carried out on the rainfall annual variables using climate oscillation indices as covariates, and uncertainties on quantile estimates are identified. It is shown that non-stationary models lead to a better fit to rainfall data. Empirical mode decomposition (EMD) is used for the long-term prediction of hydro-climatic time series. Rainfall annual time series were extended with this method for a period of 20 years. Results indicate that, within that period, annual maximum rainfall will increase by about 12 mm (or 0.6 mm/year), total annual rainfall will increase by about 200 mm (or 10 mm/year) and the number of rainy days per year will see a slight decrease by about 3 days (or 0.15 day/year).

**Keywords:** Barbados; Small island state; Rainfall; Trend analysis; Teleconnections; Climate oscillations; Frequency analysis; Empirical Mode Decomposition.

## 1 Introduction

The small islands in the Caribbean Sea are very sensitive to climate change and climate variability of large-scale ocean-atmosphere interactions. For instance, sea surface temperature (SST) in the Caribbean region has increased by 1.4 °C during the last century and is expected to continue increasing until the end of the century (Antuña-Marrero et al., 2016). With small land areas, often low elevation coasts and population and infrastructure concentrated in coastal zones, these small islands are particularly vulnerable to the impacts of climate change and variability such as rising sea level, inundations, saltwater intrusion, and shoreline changes (Nurse et al., 2014). Meteorological data are sparse in the small islands of the Caribbean Sea (Kalmarka et al., 2013) but recent global climate datasets that combine observational data with imagery on fine resolution grid cells make easier the analysis of rainfall regimes of these small islands.

Recently, a number of studies have analyzed changes and trends in precipitation indices in the small islands of the Caribbean region. In general, most studies found that trends in precipitation indices in the Caribbean are not spatially consistent and often insignificant (Karmalkar et al., 2013; Beharry et al., 2015; Jury, 2017; Dookie et al., 2019; Jury and Bernard, 2020). Stephenson et al. (2014) analyzed the changes in precipitation indices in the Caribbean region based on records spanning the 1961- 2010 and 1986-2010 intervals. Their findings suggest that changes in precipitation are generally weak. For instance, there is no significant trend in the total annual precipitation at any location at the 5% level in the interval 1961-2010. However, small increasing trends were found in the total annual precipitation, daily intensity, maximum number of consecutive dry days and heavy rainfall events particularly during the shorter period 1986–2010. Jones et al. (2016)

looked at trends across the Caribbean using two gridded data sets (CRU TS 3.21 and GPCCv5) for different regions, seasons and periods. They found no century-long trend in precipitation in the two datasets but found that most regions experienced decade-long wetter or drier periods. For the recent 1979–2012 period, they found that only a few grid cells in the Caribbean had statistically significant precipitation trends. Mohan et al. (2020), in a study focused on Barbados, used a single meteorological station over the 1969–2017 period. Statistically significant positive trends were detected in the annual total precipitation, the daily rainfall intensity index, and the total precipitation for the very wet days while the other extreme indices used showed no significant change.

End-of-century projections under different climate change scenarios predict significant warming of SST in the Caribbean region. Several studies concluded that this will lead to drier conditions in large parts of the Caribbean and Central America in the future decades (Neelin et al., 2006; Rauscher et al., 2010; Taylor et al., 2011, 2013, 2018; Campbell et al., 2011; Hall et al., 2013; Karmalkar et al., 2013; Fuentes-Franco et al., 2015). For instance, in Campbell et al. (2011), annual rainfall totals are projected to decrease by 25% to 50% for the period 2071–2100 relative to the period 1961–1990 baseline. The drying trend in the Caribbean region is expected to be more intense for the months of the wet season (Karmalkar et al., 2013; Taylor et al., 2013). A north-south gradient pattern is expected in which the southern Caribbean becomes drier than the northern Caribbean (Cambell et al., 2011; Biasutti et al., 2012). Herrera et al. (2018) argued that the recent 2013-2016 drought in the Caribbean, caused in part by a strong El Niño, was more severe due to anthropogenic warming and is likely to be a prelude to future droughts.

Several studies demonstrated the influence of the El Niño Southern Oscillation (ENSO) and the tropical North Atlantic SST on rainfall variability in the Caribbean. Positive (negative) SST anomalies in the tropical North Atlantic SST are associated with enhanced (decreased) Caribbean rainfall, and positive (negative) SST anomalies in the equatorial Pacific are associated with decreased (enhanced) rainfall (e.g. Giannini et al., 2000; Taylor et al., 2002; Spence et al., 2004; Wang et al., 2006; Anthony Chen and Taylor, 2002; Jury et al., 2007). Wu and Kirtman (2011) stressed out the relative importance of ENSO and the tropical Atlantic SST to explain rainfall variability between the early and the late rainy seasons. It was thus observed in many studies that the interannual variability of the Caribbean rainfall in the early rainy season is more closely related to the tropical North Atlantic SST anomalies, and in the late rainy season, it is more closely related to that of the equatorial Pacific and equatorial Atlantic SST anomalies (Wang et al., 2006; Taylor et al., 2011).

This study focusses on the precipitation regime in Barbados as a case study for the islands in the Caribbean region. Due to the permeable nature of the soil in Barbados, most of the island freshwater resources come from groundwater. With a large population for a small size island and a growing tourism economy, Barbados is considered as one of the most water scarce countries in the world (FAO, 2015). Recharge of groundwater aquifers in Barbados relies primarily on rainfall during the wet months (Jones and Banner, 2003). For optimal management of water resources, it is important to understand the spatial and temporal characteristics of rainfall over the island.

The present study aims first to analyze the temporal evolution of rainfall characteristics in the island of Barbados. The variables analyzed in this study are the annual and seasonal maximum rainfall, the total annual and seasonal rainfall, and the number of rainy days per year and per season. Extracted rainfall time series are analyzed for change point and trend detection. A second objective of this study is to investigate the links between ENSO and other climate oscillation indices with the rainfall variables in Barbados and construct new climate indices for Barbados based on SST anomalies. Stationary and non-stationary frequency analysis models are applied to the annual rainfall variables of this study. The identified teleconnection signals are used to select the relevant climate oscillation indices to use as covariates in the non-stationary frequency analysis along with time (representing the trend signal). This study aims also to develop long-term future predictions of the rainfall variables.

## 2 Data

Barbados is a Caribbean island located at 13°10’ N and 59° 30’ W on the east side of the Lesser Antilles of the West Indies. It is a pear-shaped small and mainly flat country that consists of a total land of 430 km$^2$ with a coastline of 97 km. It stretches about 34 km along the south-north axis and 23 km along the east-west axis (FAO, 2015). Barbados climate is hot and humid and consists of a rainy and dry season. Although it consistently rains almost all year round, the rainy season is historically and locally defined by the months of June to November in which hurricanes and downpours may occur, especially, in the August-October period. Rainfall is a very important resource as it irrigates the island through a series of small streams and fills up reservoirs. The yearly average rainfall is about 1400 mm with a significant monthly variation. Monthly rainfall can be as low as 25 mm/month during the months of January to May (FAO, 2015). Like any other Caribbean island, Barbados is affected by hurricanes. However, because of its southern location and being outside the Caribbean Sea basin, it has often been spared. Even, when this happened, the hurricanes were often reduced to their lower category levels at the time of impact. Nevertheless, the island had experienced in the past some significant hits, namely by category 5 hurricane Janet (September 1955) and more recently by Ivan (September 2004) and Dean (August 2007).

Precipitation data used in this study was obtained from the Climate Hazards group Infrared Precipitation with Stations (CHIRPS) dataset (Funk et al., 2015) available from the Climate Hazards Group at https://www.chc.ucsb.edu/data/chirps/. It combines satellite imagery with data from observation stations to produce a gridded daily, monthly and pentadal (5-days) precipitation data. CHIRPS is a near global dataset (50°S-50°N), with a high resolution of 0.05°×0.05°. It is available from 1981 to near present day and was extracted until 2018 for this study. Fig. 1 shows the spatial distribution of the gridded rainfall data of Barbados. The SST dataset used in this study is HadISST1 obtained from the Met Office Hadley Centre (Rayner et al., 2003). It provides a monthly global SST dataset on a 1°×1° grid from as early as 1871 until present.

Since the relationship between Barbados rainfall and climate is likely to differ for different seasons, seasonally stratified analysis of rainfall is performed here. The wet or rainy season is defined here by the months of May to November (MJJASON) and the dry season by the months of December to April (DJFMA). The bimodal nature of rainfall in the Caribbean region during the rainy season is largely recognized in the literature where it was observed that a relative minimum of rainfall generally occurs between July and

August (Small et al., 2007). In this study, the rainy season is separated into an early rainy season defined by the months of May-June-July (MJJ) and a late rainy season defined by the months of August-September-October-November (ASON).

From the precipitation daily data, the following variables were computed for each grid cell: annual, monthly and seasonal maximum rainfall, total annual, monthly and seasonal rainfall and number of rainy days per year, per month and per season. Overall analyzes in this study are carried out on the time series defined by the average values of the grid cells covering the island.

# 3 Methods

## 3.1 Mann-Kendall test

The test of Mann-Kendall (MK; Mann, 1945; Kendall, 1975) is a non-parametric test commonly used to detect monotonic trends in time series in hydro-climatic and environmental sciences. It has been one of the most used tests for trend detection in hydro-meteorological time series (Fu et al., 2004; Khaliq et al., 2009; Fiala et al., 2010). The main advantage of non-parametric statistical tests compared to parametric tests is that they can handle non-normally distributed and censored data, which are frequently encountered in hydro-meteorological time series (Yue et al., 2002a). The MK test is based on the *S* statistic defined by:

$$S = \sum_{i=1}^{n-1} \sum_{j=i+1}^{n} \operatorname{sgn}(x_j - x_i) \tag{1}$$

where $x$ is a data sample of size $n$, $x_i$ and $x_j$ are the data values for periods $i$ and $j$ respectively and sgn(.) is the sign function.

For large sample sizes, the $S$ statistic is approximately normally distributed and the standardized normal test statistic $Z_S$ is given by:

$$Z_S = \begin{cases} \dfrac{S-1}{\sqrt{\mathrm{Var}(S)}} & \text{if S > 0} \\ 0 & \text{if S = 0} \\ \dfrac{S+1}{\sqrt{\mathrm{Var}(S)}} & \text{if S < 0} \end{cases} \quad (2)$$

The null hypothesis that there is no trend can be rejected at a significance level of $p$ if $|Z_S| > Z_{1-p/2}$ where $Z_{1-p/2}$ can be obtained from the standard normal cumulative distribution tables.

The potential presence of positive autocorrelation in time series increases the probability of detecting trends when there is no trend (or vice versa). To cope with the impact of the serial correlation, Hamed and Rao (1998) proposed a variant of the MK test in which the variance of $S$ is modified to account for autocorrelation in the data. Following this method, the lag-1 autocorrelation is considered in this study and the modified MK is applied when it is significant.

**3.2 Theil-Sen's slope estimator**

The true magnitude of the slope of a data sample, can be estimated with the Theil-Sen's estimator (Theil, 1992; Sen, 1968) given by:

$$b = \text{median}\left(\frac{x_j - x_i}{j-i}\right) \quad \forall 1 < i < j \tag{3}$$

where $x_i$ and $x_j$ are the *i*th and *j*th observations of *x*, a sample of *n* observations. This method yields a robust estimator of the slope of a trend (Yue et al., 2002) and has been frequently used in environmental sciences (Ouarda et al., 2014).

**3.3 L-Moment ratio diagrams**

In frequency analysis, it is important to use a model that gives a good fit to the data for better accuracy of quantile estimations. L-moment ratio diagrams are useful tools to identify the distribution among candidate distributions that provide the best fit to the data. L-moments, introduced by Hosking (1990), consist of alternative statistics to classical moments to describe the shape of distributions. We denote by $\lambda_r$ the L-moment of order *r*. The dimensionless L-moment ratios, L-variation, L-skewness and L-kurtosis are analogous to the conventional coefficient of variation, skewness and kurtosis and are respectively defined by:

$$\begin{aligned} \tau_2 &= \lambda_2 / \lambda_1 \\ \tau_3 &= \lambda_3 / \lambda_2 \,. \\ \tau_4 &= \lambda_4 / \lambda_2 \end{aligned} \tag{4}$$

L-moments often need to be estimated from finite samples. Analogous sample L-moment ratios to L-moment ratios in Eq. (12) are defined by:

$$\begin{aligned} t_2 &= \ell_2 / \ell_1 \\ t_3 &= \ell_3 / \ell_2 \,. \\ t_4 &= \ell_4 / \ell_2 \end{aligned} \tag{5}$$

where $\ell_r$ is the sample L-moment of *r* order. L-moments present many advantages over conventional moments as they are able to characterize a wider range of distributions, they are more robust in the presence of outliers in the data sample and are less subject to bias in the estimation (Hosking and Wallis, 1997).

L-moment ratio diagrams, which usually plot L-kurtosis against L-skewness, provide a convenient way to represent shape characteristics of probability distributions. In such diagram, a given distribution is represented by a point if it has no shape parameter, a curve if it has one shape parameter or an area if it has two shape parameters. With this approach, all possible values of the L-skewness and L-kurtosis for a given pdf are represented in a single diagram. This diagram allows to appropriately select a distribution to fit a data sample based on the location of its sample L-moment ratios and are commonly used in hydro-climatology (see for instance Wan Zin et al., 2009; Ouarda et al., 2016; Ouarda and Charron, 2019).

### 3.4 Nonstationary frequency analysis

Frequency analysis is used here to determine the probability of occurrence of precipitation events. For that, a probability distribution function is typically fitted to data and quantiles are predicted for return periods of interest. In this study, the generalized extreme value (GEV) is used to model the maximum and total rainfall while the generalized logistic (GLO) is used to model the number of rainy days. The GEV has three parameters and is the theoretical asymptotic distribution for annual maxima. The cumulative probability function of the GEV is given by (Coles, 2001):

$$\mathrm{GEV}(x;\mu,\sigma,\kappa)=\begin{cases}\exp\left\{-\left[1+\kappa\left(\dfrac{x-\mu}{\sigma}\right)\right]^{-1/\kappa}\right\} & \text{if } k\neq 0\\ \exp\left[-\exp\left(-\dfrac{x-\mu}{\sigma}\right)\right] & \text{if } k=0\end{cases} \tag{6}$$

where $\mu$, $\sigma>0$, and $\kappa$ are the location, scale and shape parameters respectively, and $\mu-\sigma/\kappa<x<\infty$ for $\kappa>0$, $-\infty<x<\infty$ for $\kappa=0$ and $-\infty<x<\mu-\sigma/\kappa$ for $\kappa<0$. The cumulative probability function of the GLO is given by (Hosking and Wallis, 1997):

$$\mathrm{GLO}(x;\mu,\sigma,\kappa)=\begin{cases}\left\{1+\left[1-\kappa\left(\dfrac{x-\mu}{\sigma}\right)\right]^{1/\kappa}\right\}^{-1} & \text{if } k\neq 0\\ \left[1+\exp\left(-\dfrac{x-\mu}{\sigma}\right)\right]^{-1} & \text{if } k=0\end{cases} \tag{7}$$

where $\mu$, $\sigma>0$, and $\kappa$ are the location, scale and shape parameters respectively, and $\mu-\sigma/\kappa<x<\infty$ for $\kappa<0$, $-\infty<x<\infty$ for $\kappa=0$ and $-\infty<x<\mu-\sigma/\kappa$ for $\kappa>0$.

Classical statistical models used in frequency analysis assume that time series are independent and identically distributed. However, this is unrealistic in practice in a context of climate change and under the influence of large-scale oscillation phenomena. For this reason, hydrologists are increasingly using nonstationary frequency analysis models in which covariates representing trends or climate indices are introduced (see for instance El-Adlouni et al., 2007; Ouarda and El-Adlouni, 2011). In the nonstationary framework, the parameters of the distribution are conditional upon time-dependent covariates (Katz et al., 2002). These covariates can for instance represent the eventual temporal trend or climate cycles (Thiombiano et al., 2018; Ouarda et al., 2019). For the sake of simplicity, in this study, only the location parameter of the nonstationary GEV and GLO models can depend linearly on one or two climate indices:

$$\mu_t = a_0 + a_1 Y_t \tag{8}$$

$$\mu_t = a_0 + a_1 Y_t + a_2 Z_t \tag{9}$$

where *a* are the parameters to be estimated and $Y_t$ and $Z_t$ are time-dependent covariates. The assumption of the sole dependence of the location parameter on covariates has commonly been adopted in the nonstationary modeling of hydro-climatic variables (El-Adlouni and Ouarda, 2008, 2009).

The maximum likelihood method (ML) is commonly used to estimate $\theta = (\alpha_0, \alpha_1, \sigma, \kappa)$ or $\theta = (\alpha_0, \alpha_1, \alpha_2, \sigma, \kappa)$, the vector of distribution parameters. Given a data sample $x = \{\mathrm{x}_1, ..., \mathrm{x}_n\}$, the likelihood objective function is given by:

$$L_n = \prod_{t=1}^{n} f(x_t; \theta) \tag{10}$$

where *f* is the probability density function. An optimization function in Matlab is used to obtain $\hat{\theta}$, the estimator of $\theta$ that maximizes Eq. (18).

Model comparison is made here with the Akaike information criterion (AIC) and the Bayesian information criterion (BIC) given by:

$$\mathrm{AIC} = -2\ln(L_n) + 2k\,, \tag{11}$$

$$\mathrm{BIC} = -2\ln(L_n) + k\ln(n) \tag{12}$$

where $k$ is the number of parameters of the model. AIC and BIC are indicators of the goodness-of-fit of the model to the data but account also for the parsimony by penalizing more complex models involving a larger number of parameters.

Confidence intervals (CIs) for the quantile estimates are computed here with the parametric bootstrap method (Efron and Tibshirani, 1993). In this method, the parameter vector $\theta$ is initially estimated with the data sample. Then, $B$ samples of random numbers of the same size than the data sample are generated from $F^{-1}(x,\hat{\theta})$, the inverse function of the probability function. For each drawn sample, an estimate of $\theta$ is computed and quantiles are deduced. For large $B$, it is assumed that the $B$ estimated quantiles are normally distributed, and the CIs of the quantiles are computed using the variance of the $B$ quantiles.

### 3.5 Empirical mode decomposition (EMD)

EMD is an algorithm used to decompose a signal into a finite number of oscillatory modes whose frequencies are significantly apart from each other. These extracted components are labeled as intrinsic mode functions (IMF). Lee and Ouarda (2010) introduced a methodology to extend the IMFs into the future. This method has been used for the long-term prediction of hydro-climatic time series (Lee and Ouarda, 2010; 2011). This method consists in a) decompose the time series into a finite number of IMFs, b) find the significant components among them, c) fit a stochastic time series model (parametrically or nonparametrically) to the selected significant components and the residuals accordingly, d) extend the future evolution of each component from the fitted models, and e) sum up those separately modeled components. A significant test developed by Wu and Huang (2004) is used to determine if a component is statistically different from white noise.

# 4 Results and discussion

## 4.1 Statistical tests and change point analysis

The spatial distribution of the rainfall variables is illustrated in Fig. 2 with a different map for each variable. The mean value at each pixel is represented by a color corresponding to its magnitude on the color map. It can be observed that the eastern region receives more rain in intensity, quantity and frequency than the western region. The prevailing wind coming from the east, added to the presence of a moderately high mountainous regions in the center of the island (see Fig. 1), play a role in this distribution of precipitation. The time series of the mean of all the grid cells that cover the island is analyzed here for a global representation of the precipitation over the whole island.

Fig. 3 presents the annual time series for the three rainfall variables for the whole island, for a single cell located in the eastern region and a single cell in the western region to illustrate the spatial distribution. The location of the centers of the western and the eastern cells is indicated in Fig. 2. Time series for the total rainfall and the number of rainy day at the western grid cell and the eastern grid cell are highly correlated with a correlation coefficient of 0.94 and 0.83 respectively, while for the maximum rainfall they are weakly correlated with a correlation coefficient of 0.29. The eastern point has in general the most important precipitation in intensity, quantity and frequency followed by the rest of the island and finally the western point. The mean differences between the western grid cell and the eastern grid cell are 33 mm for the annual maximum rainfall, 406 mm for the total annual rainfall and 8 days for the number of rainy days by year.

Fig. 4 illustrates the seasonality of rainfall with the polar plots of the mean monthly maximum rainfall, the mean total monthly rainfall, and the mean number of rainy days per month. It can be seen from the polar plots that the rainy season spans the months of June to November. The heaviest rainfalls occur usually during the month of November for which the number of rainy days is also the smallest during the rainy season.

A multiple change point detection procedure based on Bayesian statistics (see Seidou and Ouarda (2007) for details on the method) was applied to each annual and seasonal rainfall time series with a minimum segment length of 10 years between potential change points. Results indicate that no significant changes are detected for any annual or seasonal rainfall variable for the whole island. True slopes for rainfall variables for annual and seasonal time series obtained with the Theil-Sen’s estimator are presented in Table 1. Results of the Mann-Kendall trend test reveal that no trend in annual and seasonal rainfall variables are significant at the 5% level. For the period 1981-2018 on the whole island, the annual maximum rainfall has slightly increased by 0.28 mm/year, the total annual rainfall has slightly decreased by -1.1 mm/year and the number of rainy days per year has slightly increased by 0.01 day/year. There is a decreasing trend for the overall rainy season from May to November and there is an increasing trend for the dry season for all rainfall variables. While the trends detected in this analysis may seem very moderate, it is important to identify them as they may have important impacts on the future management of water resources in the Island of Barbados. The country is already considered as one of the most water stressed countries in the world

These results are in agreement with previous studies which concluded that long-term trends are weak in most parts of the Caribbean region (Jury and Bernard, 2020; Dookie et al., 2019; Jones et al., 2016; Stephenson et al., 2014). Mohan (2020) analyzed trend in rainfall indices at a single station located on the west side of the island and found an increasing significant trend in the total annual precipitation. Our results also show an increase in the total amount for the western grid cell, but the trend is not significant. Jones et al. (2016) raised the question of why a warmer SST in the Caribbean region did not translate into wetter conditions? They suggest that the interannual variability that currently dominates the precipitation signal could explain the absence of an overall trend.

### 4.2 Influences of climate oscillations

Global SST influence on rainfall regime in Barbados is investigated here with an analysis of the 2-dimensional SST correlation map for each of the rainfall seasons. To construct the correlation maps, SST anomalies are computed at each grid cell using the HadISST1 dataset based on the normal temperature during the base period of 1981 to 2018. The correlation between the total rainfall for a given season and the SST anomalies averaged over the same season is computed at each grid cell. Fig. 5a shows that the SST in the tropical North Atlantic have a preponderant influence on the early wet rainfall season in Barbados while the influence of tropical Pacific SST is insignificant. This situation is reversed for the late rainy season where it is the equatorial Pacific SST that has a preponderant influence (Fig. 5b). The equatorial Pacific SST is also the dominant zone of influence with rainfall during the dry season (Fig. 5c).

Following this analysis, some SST indices are constructed based on the identified zones of influence. To compute the SST indices, the time series of SST anomalies are averaged over the selected key areas and the obtained time series are finally detrended. The rectangles in Fig. 5 denote two identified key areas. The SST index for the North Atlantic is denoted by $SST_{Atl}$ and is defined by the rectangle between 10°N - 21°N and 57°W - 30°W. The SST index for the equatorial Pacific index is denoted by $SST_{Pac}$ and is defined by the rectangle between 8°S - 8°N and 180°W - 120°W.

The links between low frequency climate oscillation indices which have potential influences on rainfall variables in Barbados are established using correlation analyses. Seasons at different time lags for the climate indices are considered. Seasonal climate indices with important influences on the Caribbean rainfall are used as covariates in the non-stationary models. Pearson's correlations between the annual rainfall variables and climate oscillation indices are computed. Selected climate indices used include the Southern Oscillation Index (SOI) as a measure of ENSO, the Arctic Oscillation Index (AO), the Pacific Decadal Oscillation (PDO), the Pacific North-American (PNA) pattern, the Atlantic Multidecadal Oscillation (AMO) and the Western Hemisphere Warm Pool (WHWP). Monthly climate indices are obtained from the NOAA Physical Sciences Laboratory (available at https://psl.noaa.gov/data/climateindices/list/). The climate indices were averaged for moving windows of 3 months in order to identify the seasons with the lags having the most impacts on the rainfall variables. Such approach has been carried out in different regions of the world in a number of studies (e.g. Thiombiano et al., 2018; Chandran et al., 2016). The significance of the correlations is evaluated here with the student's *t*-test at a significance level of 10%.

Figs. 6-9 show the temporal evolution of the correlation between the rainfall variables and the selected seasonal climate indices for each season respectively. The months of the seasonal index are denoted with 3 capital letters and the symbol * indicates a season that happened before the year of observed rainfall events. These seasons are especially of interest as they provide good potential predictors of the magnitude of rainfall variables.

For the early rainy season, AMO, WHWP, TNA and $SST_{Atl}$ have the strongest correlations with rainfall in Barbados. All these indices are related to SST in the tropical North Atlantic, identified as a zone of influence for the early rainy season. TNA and $SST_{Atl}$ are the best predictors with significant correlations for all rainfall variables. Both indices give similar correlation patterns and their definitions are also very similar. SOI and PNA, which are indices related to the Pacific SST, also give significant correlations when computed during winter. For the late rainy season, it is the indices SOI and $SST_{Pac}$, related to SST in the Pacific, that have the strongest correlations with the rainfall variables. AO during winter is also important. Maximum rainfall is generally uncorrelated with the climate indices unlike annual totals and the number of rainy days. For the dry season, it is the indices SOI, PDO, PNA and $SST_{Pac}$, related to the Pacific SST, that have the strongest correlations with the rainfall variables. AMO, TNA and $SST_{Atl}$ also have influences but with lags. The number of rainy days is unrelated with indices in the Pacific, unlike total and maximum precipitation, but is related to North Atlantic SST indices. For the whole year, most climate indices have significant correlations with various lags. This reflects the fact that annual rainfall consists in a mix of the subseasons. Maximum rainfall is generally uncorrelated with climate indices. The results of the teleconnection analysis can be of significant importance as they represent the basis for the development of seasonal and long-term forecasts of rainfall variables. These rainfall forecasts, even if qualitative, can have significant impacts on the management of water resources in the country.

Frequency analysis can be performed on the rainfall variables of each season, but it is chosen here to illustrate the method with the annual rainfall variables. Based on the graphs in Fig. 9, the selected indices to be used as covariates in the nonstationary model are AO(JFM) and PNA(OND*) for the maximum rainfall, AO(AMJ) and SOI(MMJ) for the total rainfall and for the number of rainy days. These indices have significant correlations with precipitation variables and precede the rainy season or occur at the beginning of the rainy season in the case of SOI(MJJ).

### 4.3 Nonstationary frequency analysis

The L-moment ratio diagram in Fig. 10 suggests that the GEV is an appropriate model for the maximum rainfall and the total rainfall and that GLO is more appropriate to model the number of rainy days. Stationary models and nonstationary models using the selected climate indices were fitted to the rainfall time series. Temporal trends are often introduced in nonstationary models, but in this case, it was shown that trends are not significant in the observed time series. On the other hand, climate indices have a strong influence on rainfall in Barbados. Table 2 presents the differences in AIC and BIC statistics between the nonstationary models and the stationary model for each variable for the whole island. These statistics show that improvements are obtained in all cases when one or two climate indices are introduced as covariates in the frequency models and that the best overall fits are obtained with two climate indices.

Fig. 11 presents the quantiles corresponding to the non-exceedance probabilities $p$ = 0.5 for the nonstationary models versus the magnitude of the climate index used as covariate in the models. For comparison purposes, the stationary model is also displayed in each figure. 95% confidence intervals of the estimated quantiles are provided using the parametric bootstrap method. Table 3 presents a comparison of the quantiles obtained for the stationary model and the nonstationary models with three cases for the value of the climate index (the minimum, the mean, and the maximum value of the historic observed climate index).

Fig. 11 and Table 3 indicate that important differences are obtained in quantiles when the information about the covariate is used. For models with two covariates, results are presented with plots of the quantiles versus both climate indices on two different axes. Fig. 12 presents the quantile corresponding to the non-exceedance probabilities $p = 0.5$ for the nonstationary models with two covariates for each rainfall variable for the whole island versus the selected seasonal climate indices used as covariates. The amplified combined effect of both covariates is clearly visible in these figures. The results of the non-stationary frequency analysis can be used directly in practice for planning and management purposes. At a given time, and given the state of low frequency climate oscillation indices of interest, the values of rainfall quantiles are adjusted and a useful estimate of the rainfall variables is provided. These estimates are conditioned on the state of climate oscillation indices and will provide a more informative picture of the risk levels (for drought or floods for instance).

### 4.4 Empirical mode decomposition

The extracted IMFs with EMD are shown in Fig. 13 for the maximum rainfall on the whole island. The components are ordered from the highest frequency component c1 to the lowest frequency component c5 which represents the long-term trend. Fig. 14

illustrates the graphical identification of the significant IMF components for the maximum rainfall using the method proposed by Wu and Huang (2004). The solid line corresponds to the 95% confidence limit for white noise. Components extracted from the observations are plotted on this graph. For a point below the confidence limit, the hypothesis that the corresponding IMF of the target series is not distinguishable from the corresponding IMF of a random noise series cannot be rejected at the selected confidence level. Individual components c2 and c3 are not significant according to the significance test, but when added together, the aggregated component becomes significant as it can be noticed in Fig. 14. For this reason, c2 + c3 is used to model the rainfall time series. The component c1 is a high frequency component that does not represent any interannual predictable climate variation and is discarded. Component c2 has a periodicity of about 5 years while c3 has a periodicity of about 10 years and they could be interpreted as a response to low frequency climate oscillations.

IMF components with extension for the next 20 years are presented in Fig. 15 for the rainfall variables for the whole year and for the rainy season. Results indicate that the annual maximum rainfall is expected to increase (by about 12 mm or 0.6 mm/year on average), the total rainfall to slightly increase (by about 200 mm or 10 mm/year on average) while the number of rainy days is expected to slightly decrease (about 3 rainy days (or 0.15 days/year on average). The result obtained for the total rainfall is thus different from the observed slope of the time series. The results are quite different for the rainy season where the maximum rainfall is expected to remain constant (slight increase by about 4 mm or 0.2 mm/year in average), the total rainfall to decrease (by about 14 mm or 0.7 mm/year in average) and the number of rainy days to decrease (by about 0.4 rainy day or 0.02

day/year). The EMD approach allows integrating information concerning the overall trend (as one of the frequencies) with information concerning the oscillatory signal of the time series and allows for a more rational extrapolation than the simple use of the overall trend.

Results for annual rainfall variables are somehow different than those obtained in other studies that predict that the total precipitation, intensity and frequency will decrease in future decades (Taylor et al., 2013). The reason may be that most studies use climate simulations based on hypothetical future $CO_2$ scenarios. EMD, on the other hand, does not use climate warming scenarios. It rather develops future predictions based on past observed data. Taylor et al. (2018), using data from the Coupled Model Intercomparison Project (CMIP5), predicted increases in mean rainfall in Barbados relative to the 1971-2000 for the 1.5°C scenario but dryer climate relative to the 1971-2000 for the 2°C and 2.5°C scenarios. The results obtained here are thus consistent with the 1.5°C scenario of Taylor et al. (2018) but differ from the results obtained here for the worst case scenarios. EMD predictions integrate information concerning past climate variability and the oscillatory effects of climate indices of interest, and should be considered as complementary information to the results provided by $CO_2$ driven climate warming scenarios. EMD predictions can have practical uses for the long-term planning of water resources in the country.

## 5 Conclusions and future work

The present work aims to study the evolution of the rainfall regime in Barbados. The high resolution rainfall data (0.05°×0.05°) used in this study was obtained from a gridded dataset combining satellite images with observational stations. The variables studied in the present work are maximum rainfall, total rainfall and the number of rainy days for annual and seasonal data. Results show that there are no sudden changes in the mean or in the slope of the studied rainfall characteristics. A slight increase in the annual maximum rainfall was observed while a slight decrease was observed in the total annual rainfall and the number of rainy days per year. However, no trends are identified to be significant over the 1981-2018 period.

A large part of rainfall variability in Barbados can be attributed to climate oscillation phenomena. Low frequency climate oscillations have significant impacts on the magnitude of the studied rainfall variables but do not seem to have a direct impact on the timing of extreme rainfall events in Barbados. For the aim of rainfall quantile estimation, it is suggested to consider nonstationary frequency analysis models in which climate indices are introduced as covariates. The AO(JFM) and PNA(OND*) indices represent adequate covariates for the maximum rainfall, while AO(AMJ) and SOI(MMJ) are adequate for the total rainfall and the number of rainy days. A stratified study of the relationship with SST revealed that the early rainy season is linked with SST in the North Atlantic and the late rainy season is linked with SST in the tropical Pacific.

This study has certain limitations in the sense that it is statistical in nature, i.e. the results obtained are not linked to physical processes. For instance, the EMD method uses past observations of precipitation to obtain forecasts. This method differs with projections obtained with coupled models under different climate change scenarios where future hypothesis about physical processes are considered. In addition, in the non-stationary frequency approach, the model outcomes provide a precipitation level associated to a probability of occurrence for a given state of the covariate. In that case, the covariate is a seasonal climate index selected based on correlations.

Future work should focus on understanding the teleconnection mechanisms that control precipitation characteristics over Barbados and adjacent regions and how the Sea Surface Temperature (SST) anomalies characteristic of different oscillation indices change the weather patterns over the whole region. Future research efforts can also adopt a nonstationary Peaks-Over-Thresholds approach to model extreme precipitation events over the region. Considering that the rainy season is composed of two subseasons (or two populations) controlled by different mechanisms during the early and late rainy season, a mixture approach for the non-stationary frequency analysis could be adopted for the computation of quantiles for the whole rainy season.


## Acknowledgments

The authors thank the Natural Sciences and Engineering Research Council of Canada (NSERC) and the Canada Research Chairs Program for funding this research. The authors are grateful to the Editor-in-Chief, Dr. Hartmut Graßl and to one anonymous reviewer for their comments which helped improve the quality of the manuscript.


## Declarations


**Funding** This work was financed by the Natural Sciences and Engineering Research Council of Canada (NSERC) and the Canada Research Chairs Program.

**Conflicts of interest** The authors declare that they have no known competing interests.

**Authors' contributions** Taha B.M.J. Ouarda: Conceptualization, Methodology, Formal analysis, Data curation, Writing, Supervision, Project administration, Funding acquisition. Christian Charron: Conceptualization, Methodology, Software, Validation, Formal analysis, Writing, Visualization.

**Availability of data and material** The rainfall data that support the findings of this study are available from the Climate Hazards Group (https://www.chc.ucsb.edu/data/chirps/). The SST dataset used in this study is HadISST1 available from the Met Office Hadley Centre at https://www.metoffice.gov.uk/hadobs/hadisst/data/download.html.

**Code availability** The code that supports the findings of this study is not available.

**Ethics approval** Not applicable.

**Consent to participate** Not applicable.

**Consent for publication** Not applicable.

## References


Anthony Chen, A., Taylor, M.A., 2002. Investigating the link between early season Caribbean rainfall and the El Niño + 1 year. International Journal of Climatology, 22(1): 87-106. doi:10.1002/joc.711.

Antuña-Marrero, J.C., Otterå, O.H., Robock, A., Mesquita, M.d.S., 2016. Modelled and oserved sea surface temperature trends for the Caribbean and Antilles. International Journal of Climatology, 36(4): 1873-1886. doi:10.1002/joc.4466.

Beharry, S.L., Clarke, R.M., Kumarsingh, K., 2015. Variations in extreme temperature and precipitation for a Caribbean island: Trinidad. Theoretical and Applied Climatology, 122(3): 783-797. doi:10.1007/s00704-014-1330-9.

Biasutti, M., Sobel, A.H., Camargo, S.J., Creyts, T.T., 2012. Projected changes in thephysical climate of the Gulf Coast and Caribbean. Climatic Change, 112(3): 819-845. doi:10.1007/s10584-011-0254-y.

Campbell, J.D., Taylor, M.A., Stephenson, T.S., Watson, R.A., Whyte, F.S., 2011. Future climate of the Caribbean from a regional climate model. International Journal of Climatology, 31(12): 1866-1878. doi:10.1002/joc.2200.

Chandran, A., Basha, G., Ouarda, T.B.M.J., 2016. Influence of climate oscillations on temperature and precipitation over the United Arab Emirates. International Journal of Climatology, 36(1): 225-235. doi:10.1002/joc.4339.

Coles, S., 2001. An introduction to statistical modeling of extreme values. Springer, London, 208 pp.

Dookie, N., Chadee, X.T., Clarke, R.M., 2019. Trends in extreme temperature and precipitation indices for the Caribbean small islands: Trinidad and Tobago. Theoretical and Applied Climatology, 136(1): 31-44. doi:10.1007/s00704-018-2463-z.

Efron, B., Tibshirani, R.J., 1993. An Introduction to the Bootstrap. Chapman & Hall, New York.

El Adlouni, S., Ouarda, T.B.M.J., 2008. Comparison of methods for estimating the parameters of the non-stationary GEV model. Revue des sciences de l'eau, 21(1): 35-50. doi:10.7202/017929ar.

El Adlouni, S., Ouarda, T.B.M.J., 2009. Joint Bayesian model selection and parameter estimation of the generalized extreme value model with covariates using birth-death Markov chain Monte Carlo. Water Resources Research, 45(6): W06403. doi:10.1029/2007wr006427.

El Adlouni, S., Ouarda, T.B.M.J., Zhang, X., Roy, R., Bobee, B., 2007. Generalized maximum likelihood estimators for the nonstationary generalized extreme value model. Water Resources Research, 43(3): W03410. doi:10.1029/2005WR004545

FAO. 2015. AQUASTAT Country Profile – Barbados. Food and Agriculture Organization of the United Nations (FAO). Rome, Italy.

Fiala, T., Ouarda, T.B.M.J., Hladný, J., 2010. Evolution of low flows in the Czech Republic. Journal of Hydrology, 393(3–4): 206-218. doi:10.1016/j.jhydrol.2010.08.018.

Fu, G., Chen, S., Liu, C., Shepard, D., 2004. Hydro-Climatic Trends of the Yellow River Basin for the Last 50 Years. Climatic Change, 65(1): 149-178. doi:10.1023/B:CLIM.0000037491.95395.bb.

Fuentes-Franco, R., Coppola, E., Giorgi, F., Pavia, E.G., Diro, G.T., Graef, F., 2015. Inter-annual variability of precipitation over Southern Mexico and Central America and its relationship to sea surface temperature from a set of future projections from CMIP5 GCMs and RegCM4 CORDEX simulations. Climate Dynamics, 45(1): 425-440. doi:10.1007/s00382-014-2258-6.

Funk, C., Peterson, P., Landsfeld, M., Pedreros, D., Verdin, J., Shukla, S., Husak, G., Rowland, J., Harrison, L., Hoell, A., Michaelsen, J., 2015. The climate hazards infrared precipitation with stations—a new environmental record for monitoring extremes. Scientific Data, 2: 150066. doi:10.1038/sdata.2015.66.

Giannini, A., Kushnir, Y., Cane, M.A., 2000. Interannual Variability of Caribbean Rainfall, ENSO, and the Atlantic Ocean. Journal of Climate, 13(2): 297-311. doi:10.1175/1520-0442(2000)013<0297:Ivocre>2.0.Co;2.

Hall, T.C., Sealy, A.M., Stephenson, T.S., Kusunoki, S., Taylor, M.A., Chen, A.A., Kitoh, A., 2013. Future climate of the Caribbean from a super-high-resolution atmospheric general circulation model. Theoretical and Applied Climatology, 113(1): 271-287. doi:10.1007/s00704-012-0779-7.

Hamed, K.H., Ramachandra Rao, A., 1998. A modified Mann-Kendall trend test for autocorrelated data. Journal of Hydrology, 204(1–4): 182-196. doi:10.1016/s0022-1694(97)00125-x.

Herrera, D.A., Ault, T.R., Fasullo, J.T., Coats, S.J., Carrillo, C.M., Cook, B.I., Williams, A.P., 2018. Exacerbation of the 2013–2016 Pan-Caribbean Drought by Anthropogenic Warming. Geophysical Research Letters, 45(19): 10,619-10,626. doi:10.1029/2018GL079408.

Hosking, J.R.M., 1990. L-Moments: Analysis and estimation of distributions using linear combinations of order statistics. Journal of the Royal Statistical Society. Series B (Methodological), 52(1): 105-124. doi:10.2307/2345653.

Hosking, J.R.M., Wallis, J.R., 1997. Regional frequency analysis: An approach based on L-Moments. Cambridge University Press, New York, 240 pp.

Jones, I.C., Banner, J.L., 2003. Hydrogeologic and climatic influences on spatial and interannual variation of recharge to a tropical karst island aquifer. Water Resources Research, 39(9). doi:10.1029/2002WR001543.

Jones, P.D., Harpham, C., Harris, I., Goodess, C.M., Burton, A., Centella-Artola, A., Taylor, M.A., Bezanilla-Morlot, A., Campbell, J.D., Stephenson, T.S., Joslyn, O., Nicholls, K., Baur, T., 2016. Long-term trends in precipitation and temperature across the Caribbean. International Journal of Climatology, 36(9): 3314-3333. doi:10.1002/joc.4557.

Jury, M., Malmgren, B.A., Winter, A., 2007. Subregional precipitation climate of the Caribbean and relationships with ENSO and NAO. Journal of Geophysical Research: Atmospheres, 112(D16). doi:10.1029/2006jd007541.

Jury, M.R., 2017. Spatial gradients in climatic trends across the southeastern Antilles 1980–2014. International Journal of Climatology, 37(15): 5181-5191. doi:10.1002/joc.5156.

Jury, M.R., Bernard, D., 2020. Climate trends in the East Antilles Islands. International Journal of Climatology, 40(1): 36-51. doi:10.1002/joc.6191.

Karmalkar, A.V., Taylor, M.A., Campbell, J., Stephenson, T., New, M., Centella, A., Benzanilla, A., Charlery, J., 2013. A review of observed and projected changes in climate for the islands in the Caribbean. Atmósfera, 26(2): 283-309. doi:10.1016/S0187-6236(13)71076-2.

Katz, R.W., Parlange, M.B., Naveau, P., 2002. Statistics of extremes in hydrology. Advances in Water Resources, 25(8–12): 1287-1304. doi:10.1016/S0309-1708(02)00056-8.

Kendall, M.G., 1975. Rank Correlation Methods. Griffin, London.

Khaliq, M.N., Ouarda, T.B.M.J., Gachon, P., 2009. Identification of temporal trends in annual and seasonal low flows occurring in Canadian rivers: The effect of short- and long-term persistence. Journal of Hydrology, 369(1-2): 183-197. doi:10.1016/j.jhydrol.2009.02.045.

Lee, T., Ouarda, T.B.M.J., 2010. Long-term prediction of precipitation and hydrologic extremes with nonstationary oscillation processes. Journal of Geophysical Research: Atmospheres, 115: D13107. doi:10.1029/2009jd012801.

Lee, T., Ouarda, T.B.M.J., 2011. Prediction of climate nonstationary oscillation processes with empirical mode decomposition. Journal of Geophysical Research: Atmospheres, 116: D06107. doi:10.1029/2010jd015142.

Mohan, S., Clarke, R.M., Chadee, X.T., 2020. Variations in extreme temperature and precipitation for a Caribbean island: Barbados (1969–2017). Theoretical and Applied Climatology. doi:10.1007/s00704-020-03157-9.

Mann, H.B., 1945. Nonparametric Tests Against Trend. Econometrica, 13(3): 245-259. doi:10.2307/1907187.

Nurse, L.A., R.F. McLean, J. Agard, L.P. Briguglio, V. Duvat-Magnan, N. Pelesikoti, E. Tompkins, and A. Webb, 2014: Small islands. In: Climate Change 2014: Impacts, Adaptation, and Vulnerability. Part B: Regional Aspects. Contribution of Working Group II to the Fifth Assessment Report of the Intergovernmental Panel on Climate Change [Barros, V.R., C.B. Field, D.J. Dokken, M.D. Mastrandrea, K.J. Mach, T.E. Bilir, M. Chatterjee, K.L. Ebi, Y.O. Estrada, R.C. Genova, B. Girma, E.S. Kissel, A.N. Levy, S. MacCracken, P.R. Mastrandrea, and L.L. White (eds.)]. Cambridge University Press, Cambridge, United Kingdom and New York, NY, USA, pp. 1613-1654.

Neelin, J.D., Münnich, M., Su, H., Meyerson, J.E., Holloway, C.E., 2006. Tropical drying trends in global warming models and observations. Proceedings of the National Academy of Sciences, 103(16): 6110-6115. doi:10.1073/pnas.0601798103.

Ouarda, T.B.M.J., Charron, C., 2019. Changes in the distribution of hydro-climatic extremes in a non-stationary framework. Scientific Reports, 9(1): 8104. doi:10.1038/s41598-019-44603-7.

Ouarda, T.B.M.J., Charron, C., Chebana, F., 2016. Review of criteria for the selection of probability distributions for wind speed data and introduction of the moment and L-moment ratio diagram methods, with a case study. Energy Conversion and Management, 124: 247-265. doi:10.1016/j.enconman.2016.07.012.

Ouarda, T.B.M.J., Charron, C., Niranjan Kumar, K., Marpu, P.R., Ghedira, H., Molini, A., Khayal, I., 2014. Evolution of the rainfall regime in the United Arab Emirates. Journal of Hydrology, 514(0): 258-270. doi:10.1016/j.jhydrol.2014.04.032.

Ouarda, T.B.M.J., El-Adlouni, S., 2011. Bayesian nonstationary frequency analysis of hydrological variables. JAWRA Journal of the American Water Resources Association, 47(3): 496-505. doi:10.1111/j.1752-1688.2011.00544.x.

Ouarda, T.B.M.J., Yousef, L.A., Charron, C., 2019. Non-stationary intensity-duration-frequency curves integrating information concerning teleconnections and climate change. International Journal of Climatology, 39(4): 2306-2323. doi:10.1002/joc.5953.

Rauscher, S.A., Kucharski, F., Enfield, D.B., 2010. The Role of Regional SST Warming Variations in the Drying of Meso-America in Future Climate Projections. Journal of Climate, 24(7): 2003-2016. doi:10.1175/2010JCLI3536.1.

Rayner, N.A., Parker, D.E., Horton, E.B., Folland, C.K., Alexander, L.V., Rowell, D.P., Kent, E.C., Kaplan, A., 2003. Global analyses of sea surface temperature, sea ice, and night marine air temperature since the late nineteenth century. Journal of Geophysical Research: Atmospheres, 108(D14). doi:10.1029/2002JD002670.

Seidou, O., Ouarda, T.B.M.J., 2007. Recursion-based multiple changepoint detection in multiple linear regression and application to river streamflows. Water Resources Research, 43(7). doi:10.1029/2006WR005021.

Sen, P.K., 1968. Estimates of the Regression Coefficient Based on Kendall's Tau. Journal of the American Statistical Association, 63(324): 1379-1389. doi:10.2307/2285891.

Small, R.J.O., Szoeke, S.P.d., Xie, S.-P., 2007. The Central American Midsummer Drought: Regional Aspects and Large-Scale Forcing. Journal of Climate, 20(19): 4853-4873. doi:10.1175/jcli4261.1.

Spence, J.M., Taylor, M.A., Chen, A.A., 2004. The effect of concurrent sea-surface temperature anomalies in the tropical Pacific and Atlantic on Caribbean rainfall. International Journal of Climatology, 24(12): 1531-1541. doi:10.1002/joc.1068.

Stephenson, T. S., Vincent, L. A., Allen, T., Van Meerbeeck, C. J., McLean, N., Peterson, T. C., . . . Trotman, A. R. (2014). Changes in extreme temperature and precipitation in the Caribbean region, 1961–2010. International Journal of Climatology, 34(9), 2957-2971. doi:10.1002/joc.3889

Taylor, M.A., Clarke, L.A., Centella, A., Bezanilla, A., Stephenson, T.S., Jones, J.J., Campbell, J.D., Vichot, A., Charlery, J., 2018. Future Caribbean Climates in a World of Rising Temperatures: The 1.5 vs 2.0 Dilemma. Journal of Climate, 31(7): 2907-2926. doi:10.1175/jcli-d-17-0074.1.

Taylor, M.A., Enfield, D.B., Chen, A.A., 2002. Influence of the tropical Atlantic versus the tropical Pacific on Caribbean rainfall. Journal of Geophysical Research: Oceans, 107(C9): 10-1-10-14. doi:10.1029/2001jc001097.

Taylor, M.A., Stephenson, T.S., Owino, A., Chen, A.A., Campbell, J.D., 2011. Tropical gradient influences on Caribbean rainfall. Journal of Geophysical Research: Atmospheres, 116(D21). doi:10.1029/2010JD015580.

Taylor, M.A., Whyte, F.S., Stephenson, T.S., Campbell, J.D., 2013. Why dry? Investigating the future evolution of the Caribbean Low Level Jet to explain projected Caribbean drying. International Journal of Climatology, 33(3): 784-792. doi:10.1002/joc.3461.

Theil, H., 1992. A Rank-Invariant Method of Linear and Polynomial Regression Analysis. In: Raj, B., Koerts, J. (Eds.), Henri Theil's Contributions to Economics and Econometrics. Advanced Studies in Theoretical and Applied Econometrics. Springer Netherlands, pp. 345-381. doi:10.1007/978-94-011-2546-8_20.

Thiombiano, A.N., St-Hilaire, A., El Adlouni, S.-E., Ouarda, T.B.M.J., 2018. Nonlinear response of precipitation to climate indices using a non-stationary Poissongeneralized Pareto model: case study of southeastern Canada. International Journal of Climatology, 38(S1): e875-e888. doi:10.1002/joc.5415.

Wan Zin, W.Z., Jemain, A.A., Ibrahim, K., 2009. The best fitting distribution of annual maximum rainfall in Peninsular Malaysia based on methods of L-moment and LQ-moment. Theoretical and Applied Climatology, 96(3): 337-344. doi:10.1007/s00704-008-0044-2.

Wang, C., Enfield, D.B., Lee, S.-k., Landsea, C.W., 2006. Influences of the Atlantic Warm Pool on Western Hemisphere Summer Rainfall and Atlantic Hurricanes. Journal of Climate, 19(12): 3011-3028. doi:10.1175/jcli3770.1.

Wu, Z., Huang, N.E., 2004. A study of the characteristics of white noise using the empirical mode decomposition method. Proceedings of the Royal Society of London. Series A: Mathematical, Physical and Engineering Sciences, 460(2046): 1597-1611. doi:doi:10.1098/rspa.2003.1221.

Wu, R., Kirtman, B.P., 2011. Caribbean Sea rainfall variability during the rainy season and relationship to the equatorial Pacific and tropical Atlantic SST. Climate Dynamics, 37(7): 1533-1550. doi:10.1007/s00382-010-0927-7.

Yue, S., Pilon, P., Cavadias, G., 2002. Power of the Mann-Kendall and Spearman's rho tests for detecting monotonic trends in hydrological series. Journal of Hydrology, 259(1-4): 254-271. doi:10.1016/S0022-1694(01)00594-7.

Table 1. Theil-Sen's slopes for annual and monthly time series.

| Period | Maximum rainfall (mm) | | | Total rainfall (mm) | | | Number of rainy days (day) | | |
|---|---|---|---|---|---|---|---|---|---|
| | West | East | Island | West | East | Island | West | East | Island |
| Annual | 0.11 | 0.14 | 0.28 | 0.27 | -0.53 | -1.09 | 0.00 | 0.00 | 0.01 |
| Early rainy season (MJJ) | -0.11 | -0.19 | -0.12 | 0.12 | 0.53 | 0.30 | 0.00 | -0.05 | -0.05 |
| Late rainy season (ASON) | -0.18 | -0.06 | -0.02 | -0.42 | -0.87 | -1.01 | 0.00 | 0.00 | 0.01 |
| Rainy season (MJJASON) | -0.01 | -0.12 | -0.08 | -0.25 | -1.42 | -1.40 | 0.00 | -0.08 | -0.09 |
| Dry season (DJFMA) | 0.22 | 0.69 | 0.63 | 0.92 | 1.90 | 1.15 | 0.05 | 0.08 | 0.07 |

Table 2. Differences in AIC and BIC statistics between the nonstationary models and the stationary model applied to each variable for the whole island.

| Model | Δ AIC | Δ BIC |
|---|---|---|
| Maximum rainfall | | |
| $\mathrm{GEV}(\mu_t = a_0 + a_1\mathrm{AO}_t, \sigma, \kappa)$ | -5.6 | -3.9 |
| $\mathrm{GEV}(\mu_t = a_0 + a_1\mathrm{PNA}_t, \sigma, \kappa)$ | -4.7 | -3.1 |
| $\mathrm{GEV}(\mu_t = a_0 + a_1\mathrm{AO}_t + a_2\mathrm{PNA}_t, \sigma, \kappa)$ | -11.3 | -8.1 |
| Total rainfall | | |
| $\mathrm{GEV}(\mu_t = a_0 + a_1\mathrm{AO}_t, \sigma, \kappa)$ | -9.5 | -7.9 |
| $\mathrm{GEV}(\mu_t = a_0 + a_1\mathrm{SOI}_t, \sigma, \kappa)$ | -11.7 | -10.1 |
| $\mathrm{GEV}(\mu_t = a_0 + a_1\mathrm{AO}_t + a_2\mathrm{SOI}_t, \sigma, \kappa)$ | -32.2 | -28.9 |
| Number of rainy days | | |
| $\mathrm{GLO}(\mu_t = a_0 + a_1\mathrm{AO}_t, \sigma, \kappa)$ | -7.6 | -6.0 |
| $\mathrm{GLO}(\mu_t = a_0 + a_1\mathrm{SOI}_t, \sigma, \kappa)$ | -7.9 | -6.3 |
| $\mathrm{GLO}(\mu_t = a_0 + a_1\mathrm{AO}_t + a_2\mathrm{SOI}_t, \sigma, \kappa)$ | -14.6 | -11.3 |

Table 3. Quantiles for different return periods of interest with the stationary model and the nonstationary model applied to each rainfall variable for the whole island. For each quantile, the confidence intervals are indicated in square brackets.

| Variable | Return period | Stationary model | Nonstationary model | | |
|---|---|---|---|---|---|
| | | | AO (JFM) | | |
| | | | -2.23 | 0.01 | 2.64 |
| Maximum rainfall | 2 | 81 [77 - 86] | 94 [84 - 104] | 81 [76 - 85] | 66 [56 - 77] |
| | 5 | 94 [88 - 100] | 106 [94 - 117] | 93 [86 - 99] | 79 [67 - 90] |
| | 10 | 102 [94 - 110] | 114 [101 - 126] | 101 [92 - 109] | 87 [73 - 100] |
| | 20 | 110 [99 - 121] | 122 [105 - 138] | 109 [96 - 122] | 94 [78 - 112] |
| | 50 | 119 [103 - 136] | 132 [109 - 160] | 119 [100 - 146] | 104 [82 - 131] |
| | 100 | 125 [105 - 149] | 140 [112 - 183] | 126 [102 - 169] | 112 [84 - 152] |
| | | | SOI (MJJ) | | |
| | | | -2.03 | 0.07 | 1.70 |
| Total rainfall | 2 | 1111 [1061 - 1176] | 915 [748 - 1014] | 1109 [801 - 1032] | 1260 [1060 - 1155] |
| | 5 | 1262 [1196 - 1325] | 1043 [853 - 1137] | 1236 [908 - 1158] | 1387 [1167 - 1284] |
| | 10 | 1346 [1266 - 1416] | 1117 [908 - 1215] | 1311 [959 - 1239] | 1462 [1215 - 1369] |
| | 20 | 1417 [1309 - 1513] | 1182 [957 - 1305] | 1375 [1008 - 1330] | 1526 [1253 - 1477] |
| | 50 | 1497 [1348 - 1635] | 1256 [1005 - 1447] | 1450 [1057 - 1478] | 1601 [1290 - 1633] |
| | 100 | 1548 [1367 - 1752] | 1306 [1033 - 1558] | 1500 [1077 - 1591] | 1651 [1309 - 1759] |
| | | | AO (AMJ) | | |
| | | | -0.85 | 0.09 | 1.04 |
| Number of rainy days | 2 | 64 [61 - 67] | 72 [74 - 100] | 64 [73 - 95] | 56 [67 - 78] |
| | 5 | 71 [67 - 74] | 78 [80 - 106] | 70 [78 - 101] | 62 [73 - 85] |
| | 10 | 75 [70 - 80] | 82 [83 - 110] | 74 [81 - 105] | 66 [76 - 90] |
| | 20 | 80 [73 - 88] | 86 [87 - 117] | 78 [85 - 111] | 70 [79 - 96] |
| | 50 | 86 [76 - 102] | 92 [90 - 128] | 84 [89 - 123] | 76 [82 - 111] |
| | 100 | 91 [78 - 114] | 97 [93 - 143] | 89 [91 - 139] | 80 [85 - 127] |

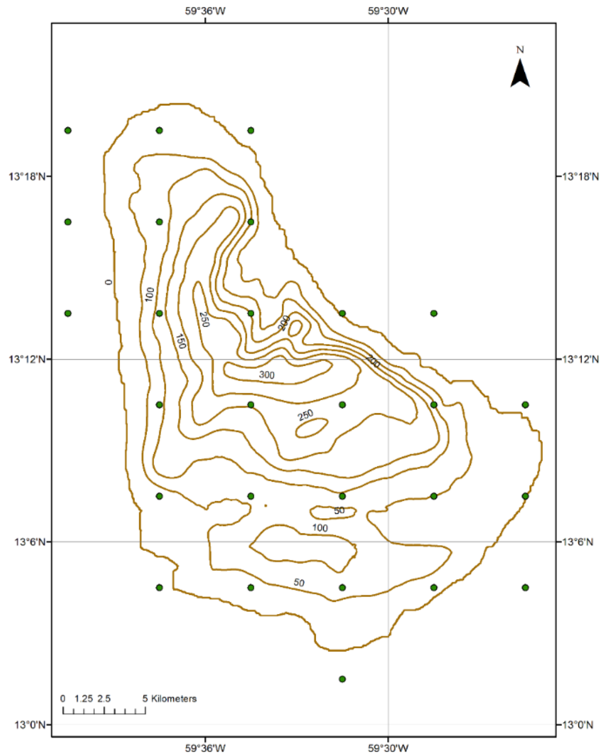


Figure 1. Topographic map of Barbados and grid cell centers for the CHIRPS dataset.

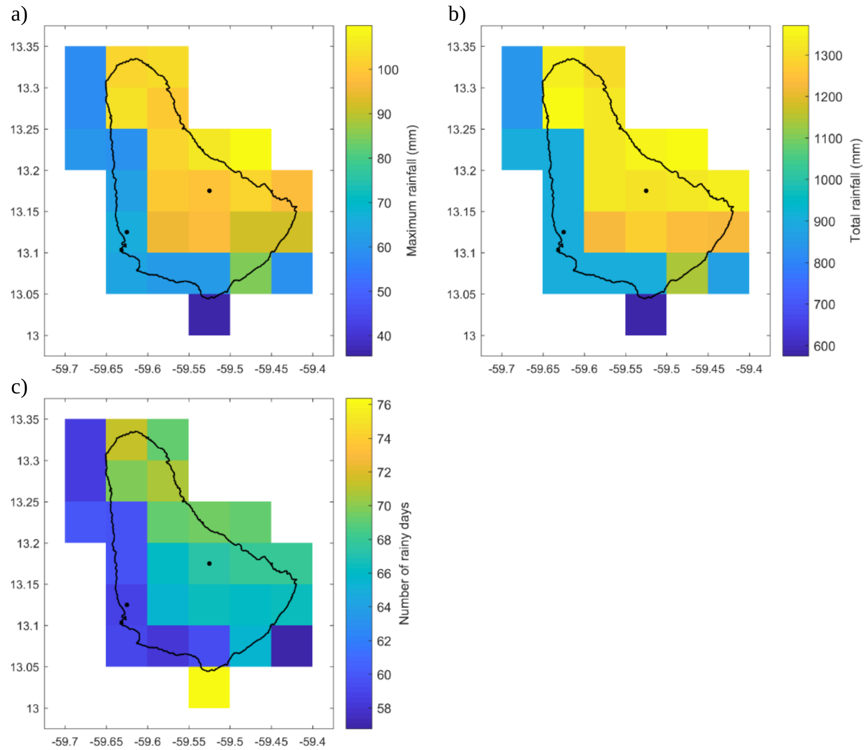


Figure 2. Means of annual maximum rainfall, total annual rainfall, and number of rainy days per year at each grid cell. The dots indicate the centers of the eastern and western grid cells analysed.

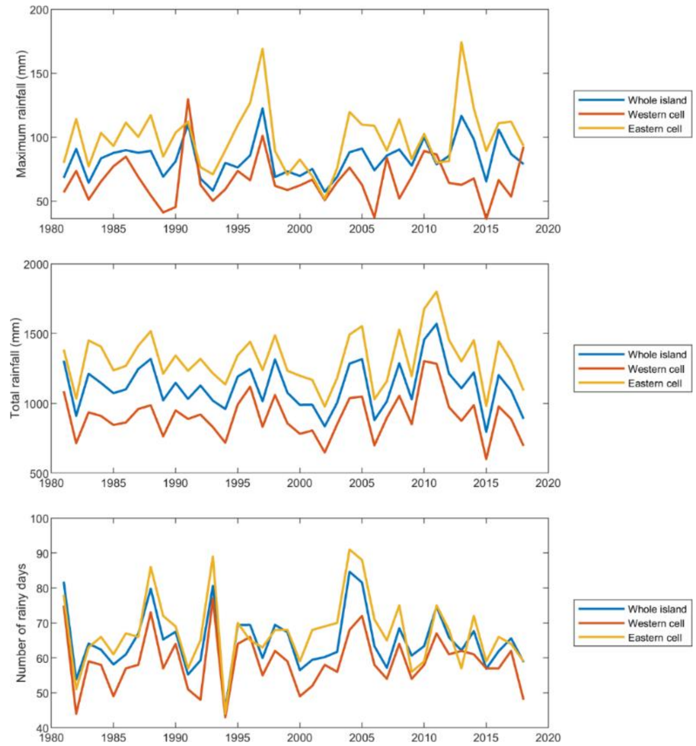


Figure 3. Annual time series for all grid cells within the island (whole island), for the western grid cell, and for the eastern grid cell.

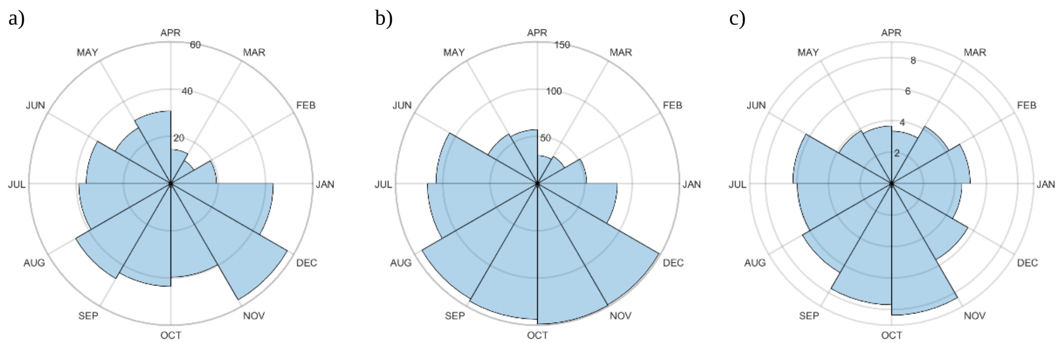


Figure 4. Mean monthly maximum rainfall (a), mean total monthly rainfall (b) and mean number of rainy days per month (c).

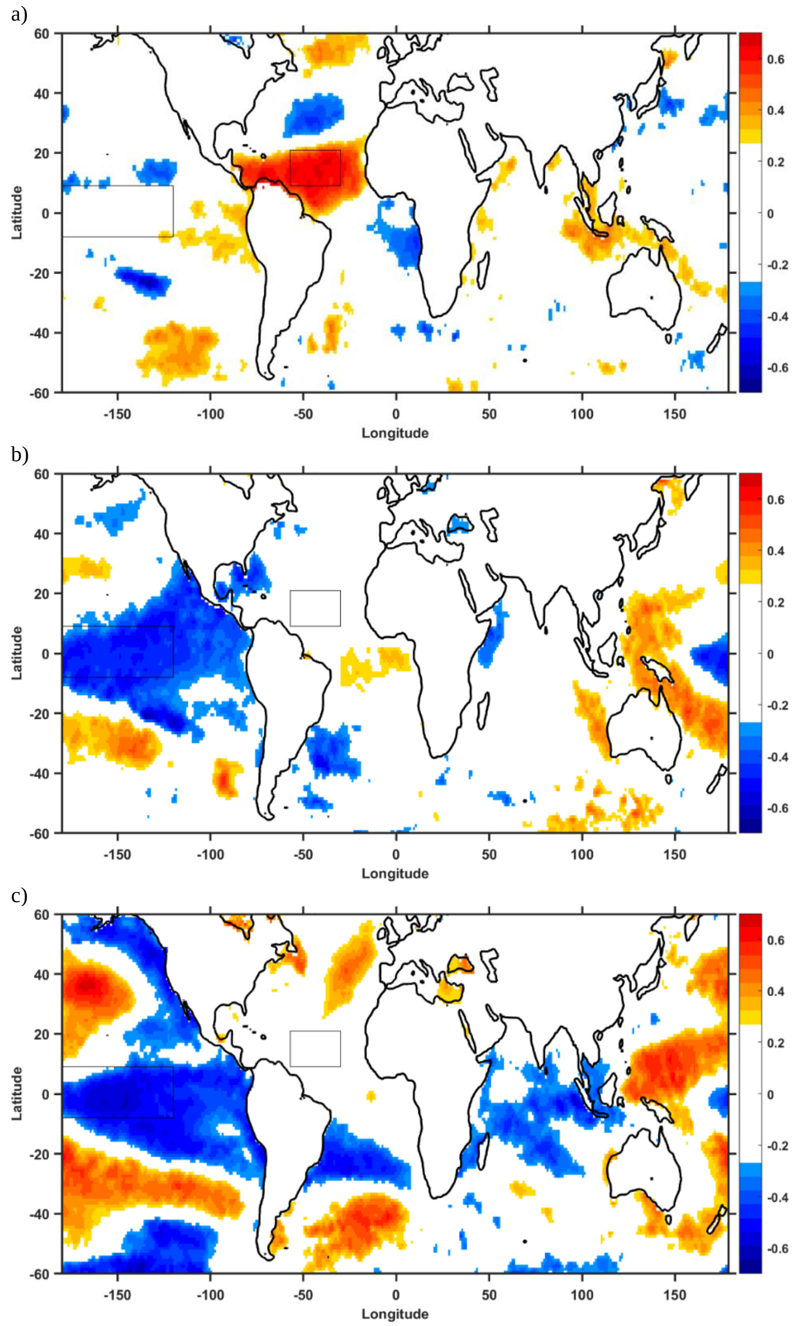


Figure 5. Maps of correlation coefficients between total annual rainfall for the early rainy season (MJJ) (a), the late rainy season (ASON) (b) and the dry season (DJFMA) (c), and sea surface temperatures during the same periods. The rectangles denote zones with preponderant influences. White areas represent locations with insignificant correlation.

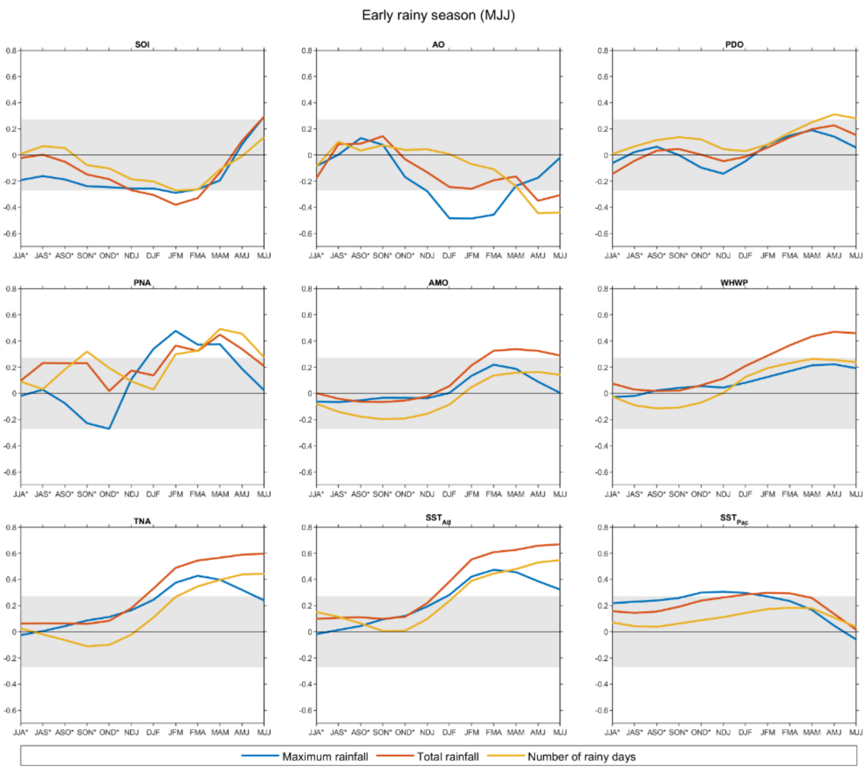


Figure 6. Seasonal temporal evolution of the correlation between the annual rainfall variables for the early rainy season and prevailing climate indices. The symbol * indicates a season before the year of the observed rainfall events. Correlations beyond the shaded area are significant at a 10% level.

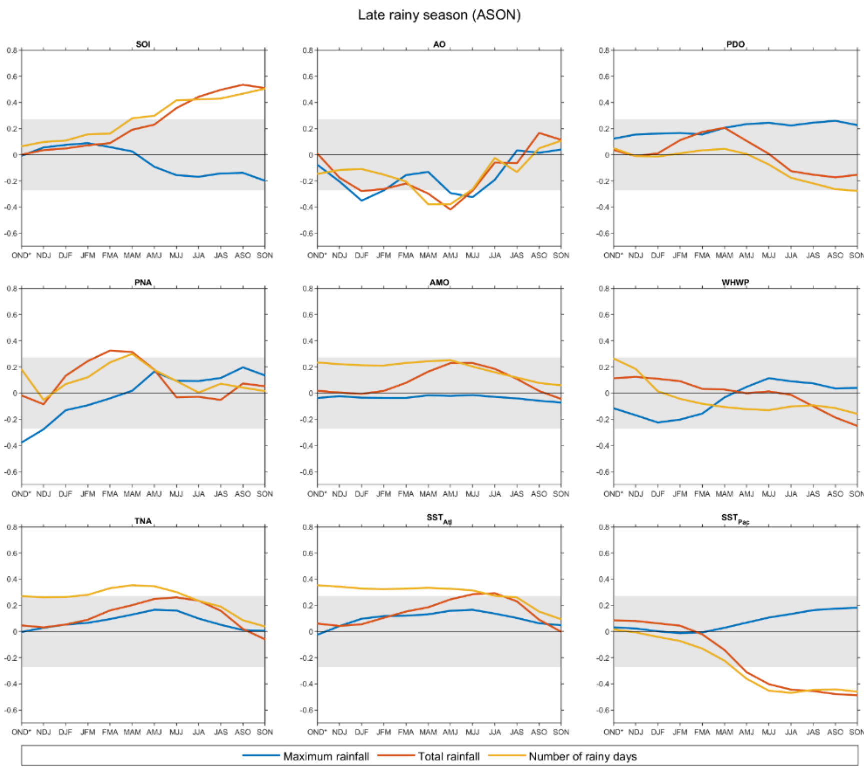


Figure 7. Seasonal temporal evolution of the correlation between the annual rainfall variables for the late rainy season and prevailing climate indices. The symbol * indicates a season before the year of the observed rainfall events. Correlations beyond the shaded area are significant at a 10% level.

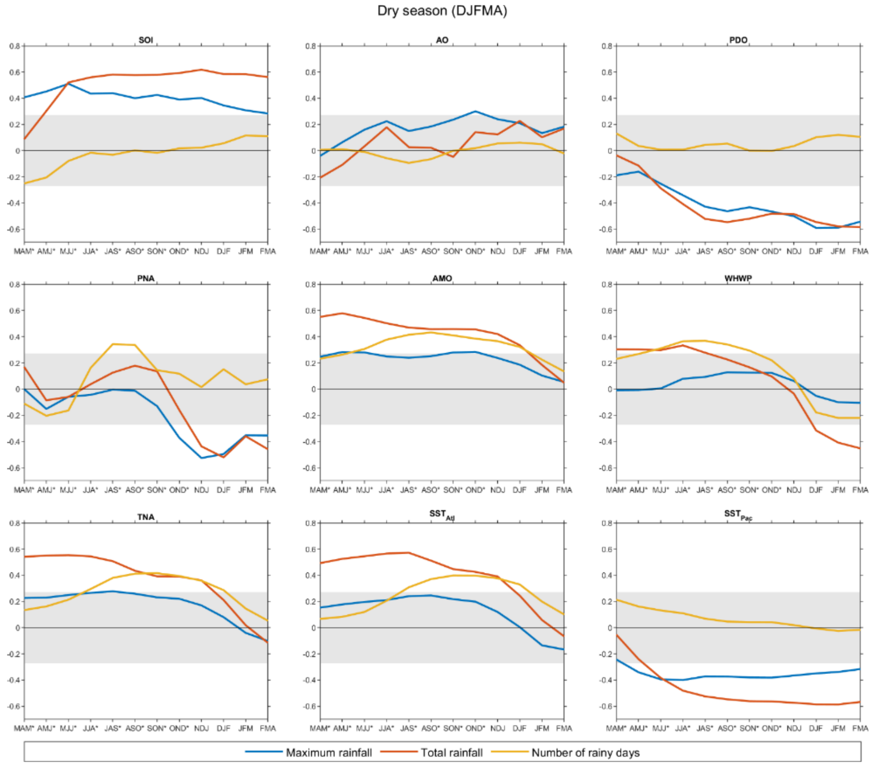


Figure 8. Seasonal temporal evolution of the correlation between the annual rainfall variables for the dry season and prevailing climate indices. The symbol * indicates a season before the year of the observed rainfall events. Correlations beyond the shaded area are significant at a 10% level.

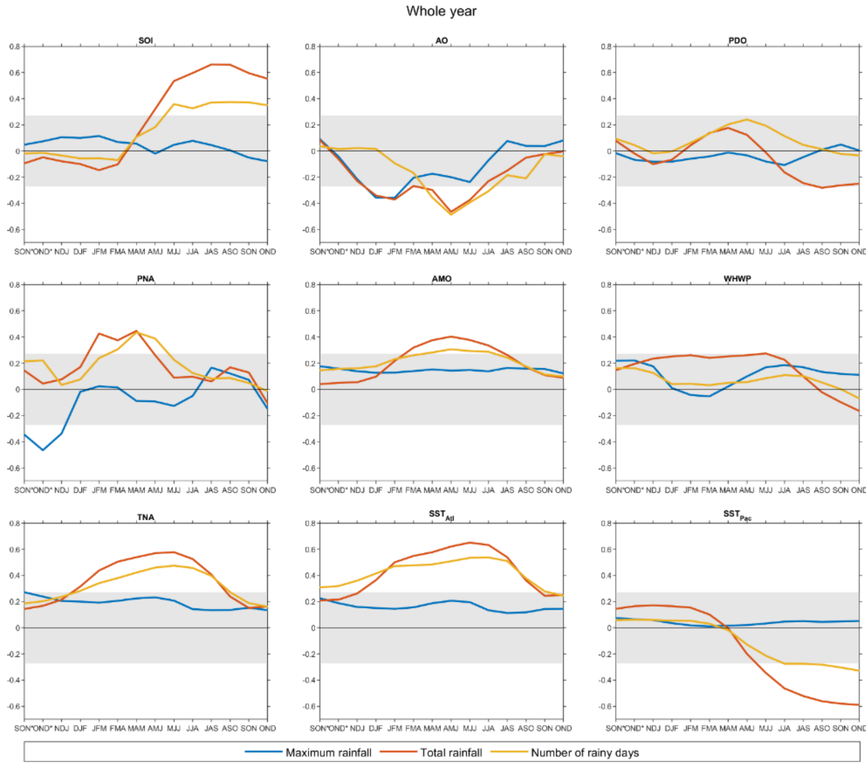


Figure 9. Seasonal temporal evolution of the correlation between the annual rainfall variables for the whole year and prevailing climate indices. The symbol * indicates a season before the year of the observed rainfall events. Correlations beyond the shaded area are significant at a 10% level.

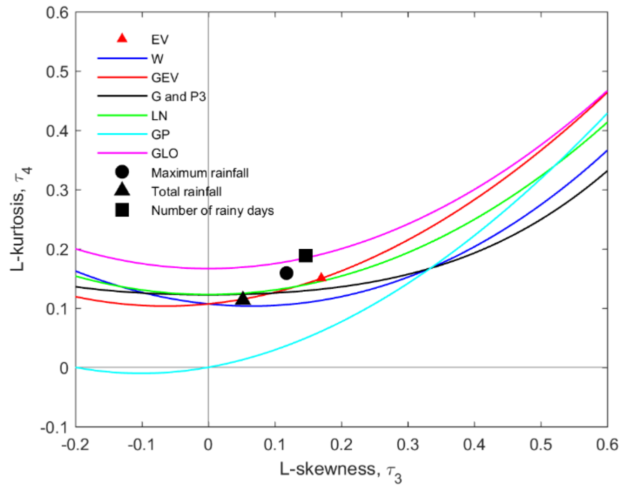


Figure 10. L-moment ratio diagram with selected theoretical pdfs. The locations of the sample L-moments of the annual time series for the island are represented by the circle, triangle and rectangle symbols.

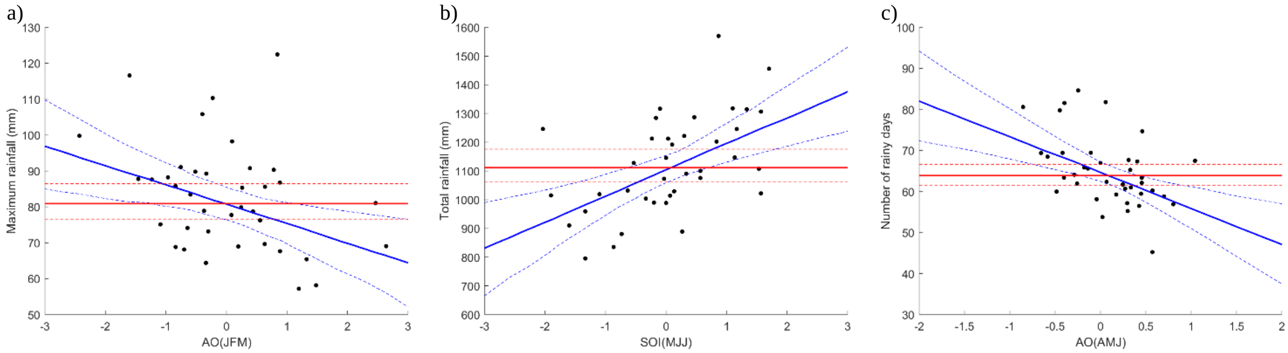


Figure 11. Quantiles corresponding to the non-exceedance probabilities $p$ = 0.5 for the nonstationary model (blue line) versus the magnitude of the selected seasonal climate index. The quantiles for the stationary model (red line) are also displayed for comparison purposes. 95% confidence intervals around the quantiles are displayed with dotted lines. Black dots represent the observations.

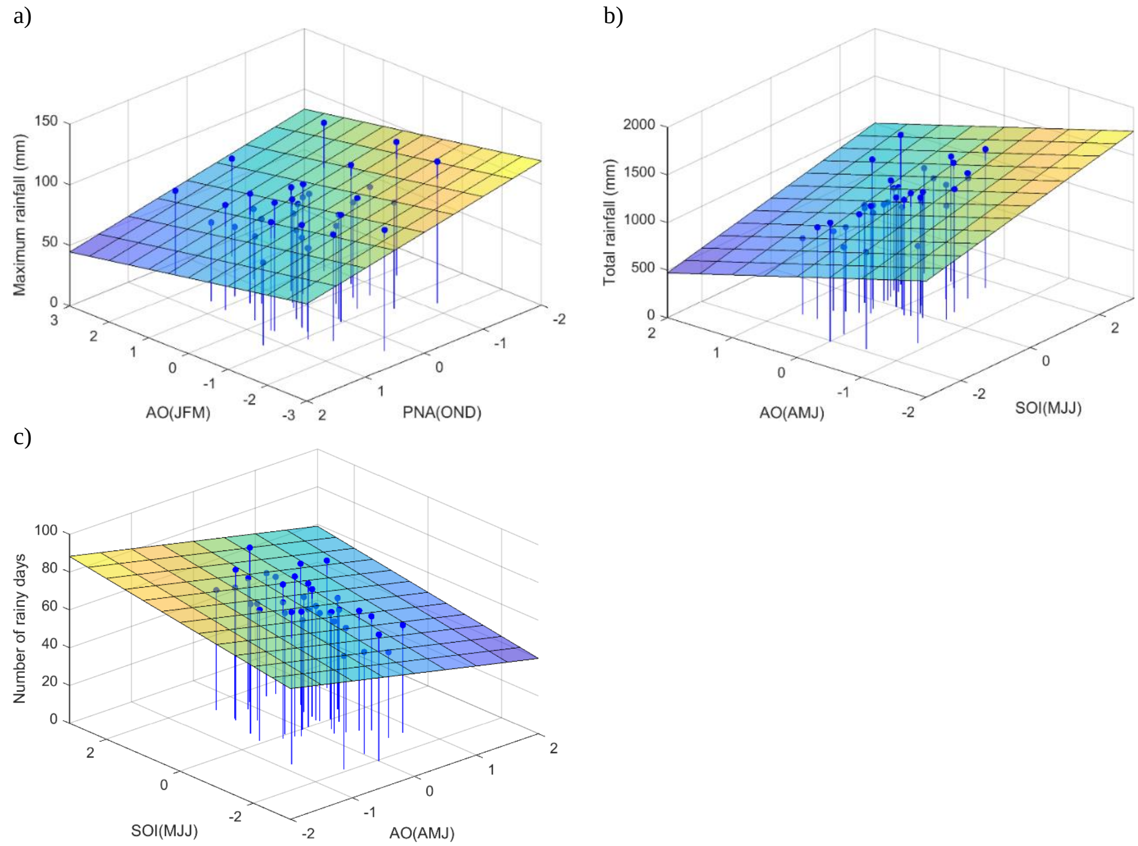


Figure 12. Quantile corresponding to the non-exceedance probabilities $p = 0.5$ for the nonstationary model with two covariates versus the magnitudes of the selected seasonal climate indices. Blue stems represent the observations.

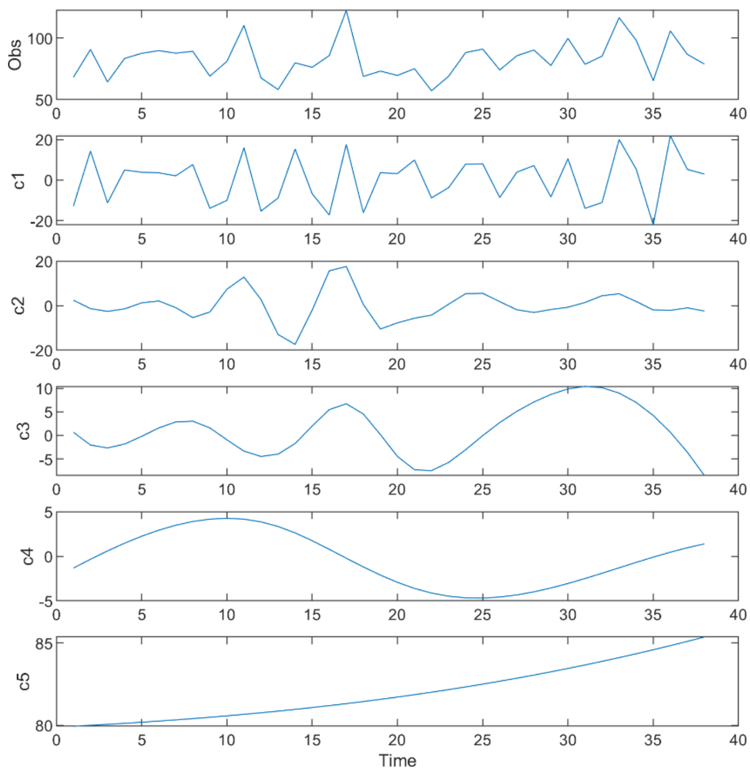


Figure 13. Observed time series of the maximum rainfall and the extracted components with EMD (c1 to c5).

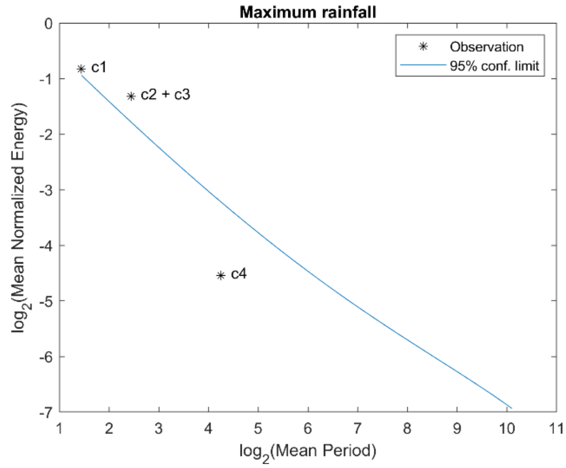


Figure 14. Significance test with 95% confidence limit. * denote the location corresponding to an IMF component. For components below the confidence limit, the hypothesis that the corresponding IMF of the target series is not distinguishable from the corresponding IMF of a random noise series cannot be rejected at the confidence level.

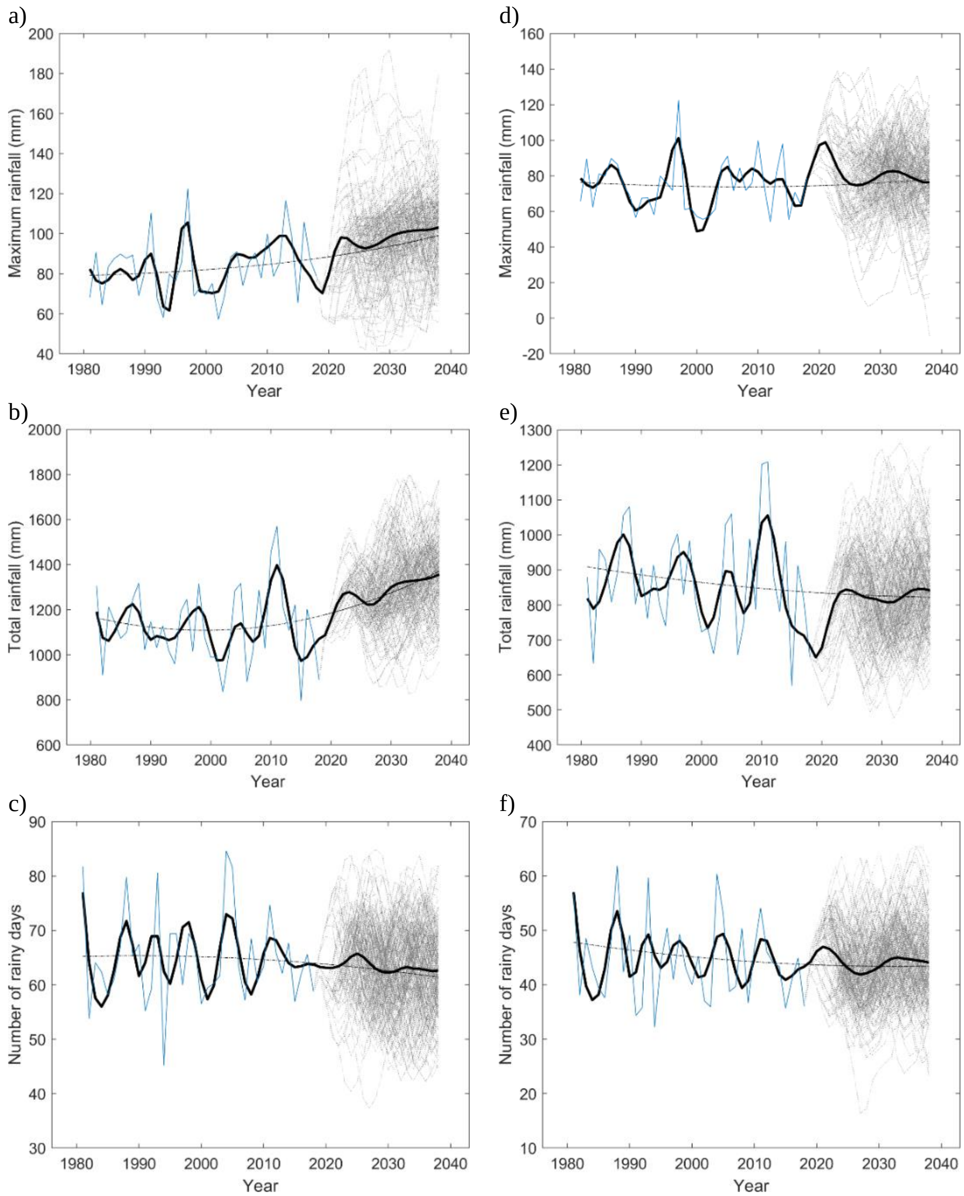


Figure 15. IMF components with extension for the next 20 years for the annual rainfall variables for the whole year (a-c) and the rainy season (d-f). The solid blue line represents the observations; the thick black solid line shows the selected IMF components and the mean of the generated 200 realizations for the extended 20 years; the grey dotted lines represent the 200 realizations; and the dashed line represents the last IMF component (the overall trend)